Glacial-interglacial vegetation dynamics in South Eastern Africa coupled to sea surface temperature variations in the Western Indian Ocean

L. M Dupont, T. Caley, J.-H. Kim, I. Castañeda, B. Malaizé, J. Giraudeau

Clim. Past, 7, 1209–1224, 2011
www.clim-past.net/7/1209/2011/
doi:10.5194/cp-7-1209-2011

Climate of the Past

Glacial-interglacial vegetation dynamics in South Eastern Africa coupled to sea surface temperature variations in the Western Indian Ocean

L. M. Dupont[1], T. Caley[2], J.-H. Kim[3], I. Castañeda[3,*], B. Malaizé[2], and J. Giraudeau[2]

[1]MARUM Center for Marine Environmental Sciences, University of Bremen, Germany
[2]Université de Bordeaux 1, CNRS, UMR 5805 EPOC, France
[3]NIOZ Royal Netherlands Institute for Sea Research, Department of Marine Organic Biogeochemistry, Texel, The Netherlands
[*]now at: Department of Geoscience, University of Massachusetts Amherst, Amherst, MA 01002, USA

Received: 28 June 2011 – Published in Clim. Past Discuss.: 6 July 2011
Revised: 20 September 2011 – Accepted: 26 September 2011 – Published: 9 November 2011

Abstract. Glacial-interglacial fluctuations in the vegetation of South Africa might elucidate the climate system at the edge of the tropics between the Indian and Atlantic Oceans. However, vegetation records covering a full glacial cycle have only been published from the eastern South Atlantic. We present a pollen record of the marine core MD96-2048 retrieved by the Marion Dufresne from the Indian Ocean ~120 km south of the Limpopo River mouth. The sedimentation at the site is slow and continuous. The upper 6 m (spanning the past 342 Ka) have been analysed for pollen and spores at millennial resolution. The terrestrial pollen assemblages indicate that during interglacials, the vegetation of eastern South Africa and southern Mozambique largely consisted of evergreen and deciduous forests. During glacials open mountainous scrubland dominated. Montane forest with *Podocarpus* extended during humid periods was favoured by strong local insolation. Correlation with the sea surface temperature record of the same core indicates that the extension of mountainous scrubland primarily depends on sea surface temperatures of the Agulhas Current. Our record corroborates terrestrial evidence of the extension of open mountainous scrubland (including fynbos-like species of the high-altitude Grassland biome) for the last glacial as well as for other glacial periods of the past 300 Ka.

Correspondence to: L. M. Dupont
(dupont@uni-bremen.de)

1 Introduction

South Africa lies at the edge of the tropics between the Indian and Atlantic Oceans. Today, only the tip of South Africa reaches into the winter rain zone touched by the circum-Antarctic Westerlies at their northernmost winter position. The eastern part of South Africa presently has a tropical summer rain climate strongly depending on the sea surface temperatures (SSTs) of the Southwest Indian Ocean and the influence of the Agulhas Current (e.g. Jury et al., 1993; Tyson and Preston-Whyte, 2000).

There has been a long standing debate over how South African climate and vegetation changed through the Pleistocene glacial-interglacial cycles. Some authors advocate a shift of the winter rainfall area northwards during glacial times but differ about the amplitude of that shift (e.g. Heine, 1982; Stuut et al., 2004; Shi et al., 2001; Chase, 2010). Others argue that most of South Africa remained under summer rain influence (Lee-Thorp and Beaumont, 1995; Partridge et al., 1999), even including the southern Cape (Bar-Matthews et al., 2010). See Chase and Meadows (2007) and Gasse et al. (2008) and references therein for the full discussion. Not only are the latitudinal position, intensity, and influence of the westerly storm tracks – and with them the extent of the summer rainfall area – insufficiently clarified, but also the impact of local versus Northern Hemisphere insolation on the climate of South Africa is largely unknown. The age model of the Tswaing Crater sequence (Partridge et al., 1997; Kirsten et al., 2007) is tuned to precession and cannot be

Published by Copernicus Publications on behalf of the European Geosciences Union.

stated as independent evidence for the impact of local insolation, which is doubted for the Holocene (Chase et al., 2010). The debate is thus fuelled by the lack of good records to address the glacial-interglacial climate cycle of land-cover change in Southern Africa. Even for the last Glacial, the terrestrial evidence is fragmentary, poorly dated or contradictory. Records integrating a full glacial-interglacial cycle or spanning more than one climate cycle are only covered by marine cores.

Yet, understanding fluctuations in vegetation and land-cover – which have shaped the environment of early humans (e.g. Marean et al., 2007; Wadley, 2007; Chase, 2010) – is critical as they are related to globally important systems such as the Agulhas and Benguela Currents, the latitude of the Subtropical Front, and the position of the sub-tropical high-pressure systems in the Southern Hemisphere. Furthermore, vegetation records can be used to validate results from earth system dynamic vegetation models of high or intermediate complexity.

In the present paper, we focus on the regional development of the vegetation of south Mozambique and the north-east corner of South Africa since 350 Ka. We study vegetation change and SST estimates (Caley et al., 2011) over several glacial-interglacial cycles to better understand the driving forces of land-cover variations in the region using sediments of a marine core retrieved near the mouth of the Limpopo River. The glacial-interglacial vegetation variability in the marine core is compared to the pollen records of Wonderkrater (Scott, 1982a; Scott et al., 2003) and the Tswaing Crater (Scott, 1999; Scott and Tackeray, 1987) in South Africa and to the pollen record of Lake Tritrivakely on Madagascar (Gasse and Van Campo, 1998, 2001).

At this stage we do not attempt to compare with the records of Lake Malawi (DeBusk, 1998; Cohen et al., 2007; Beuning et al., 2011), Lake Masoko (Vincens et al., 2007), or Kashiru (Bonnefille and Riollet, 1988), which are situated too far north to be used as a guide for the region and are, therefore, beyond the scope of this paper. A more comprehensive review of vegetation changes in Africa over several climatic cycles is given in Dupont (2011).

2 Topography and modern climate

Extensive lowlands stretch north of the site intersected by the floodplains of the Limpopo and the Changane Rivers (Fig. 1). The floodplain soils of the Changane River are salty (Kersberg, 1985, 1996). West of Maputo, the relief rises to the central plateau of southern Africa. The Great Escarpment forms here the northern part of the Drakensberg (up to over 2000 m a.s.l.). Between the escarpment and the coast lies a N-S oriented low ridge, the Lebombos hills (100–500 m a.s.l.).

The average annual temperature ranges from 16 °C on the central plateau to 24 °C in the lowland area. Lowlands are devoid of frosts, but the highland can have severe frosts during clear winter nights (Kersberg, 1996). Average annual precipitation ranges from 1400 mm in the mountains to 600 mm in the lowlands. Rain falls mostly in summer (November to March). Because of the relief of the Great Escarpment, the temperature and rainfall contours are N-S directed. Along the coast rain is more frequent. The warm waters of the Agulhas Current system bring warm and humid air over the lowland into the mountains of the Escarpment. Rainfall during late summer in the region increases with warmer sea surface temperatures (SST) of the Agulhas Current. However, rainfall diminishes when the SST of the western Southwest Indian Ocean decrease (Jury et al., 1993; Reason and Mulenga, 1999).

The area lies in the transition between tropical and subtropical climate, just south of the subtropical ridge between the southern Hadley and the Ferrel cell (Tyson and Preston-Whyte, 2000). Most of the year, surface airflow is from east to west and stronger during summer. During winter the average wind direction turns southwest in June to northeast in September, but winds tend to be weak. The topographic configuration of the high interior, the escarpment and the coastal lowland creates coastal shallow low pressure cells associated with Bergwinds blowing down the mountains in an offshore direction (Tyson and Preston-Whyte, 2000). On a daily basis, mountain winds blow offshore by night (land breeze) and onshore by day (sea breeze).

On days without rain, stable layers at about 500 hPa and 700 hPa develop over southern Africa. Between these stable layers dust and aerosols can be trapped, re-circulated over the continent for days and finally exported over large distances over the oceans to the Atlantic but mainly to the Indian Ocean (>75 %) (Tyson and Preston-Whyte, 2000). However, the transport takes place above the marine boundary layer and is thus of little consequence for the pollen delivery to our marine site close to the coast.

3 Modern vegetation

The vegetation in the region is very varied (Fig. 1) and is classified into as many as five different phytogeographical regions (phytochoria after White, 1983); two tropical phytochoria, the Zambezian interior and the Zanzibar-Inhambane coastal region; two tropical-subtropical ones, the Highveld and the coastal Tongaland-Pondoland region; and one belonging to the Afromontane region (White, 1983). The natural vegetation ranges from closed forest to dry scrubland and from alpine open grassland to semi-evergreen lowland forest. Along the rivers, wet forest alternates with floodplain savannahs and herb communities. However, most of the floodplain is now under cultivation. The saline soils along the Changane River carry halophytic plants such as *Arthrocneum* and *Atriplex* of the Chenopodiaceae family. Seasonally flooded flat depressions east of the Changane River bear a

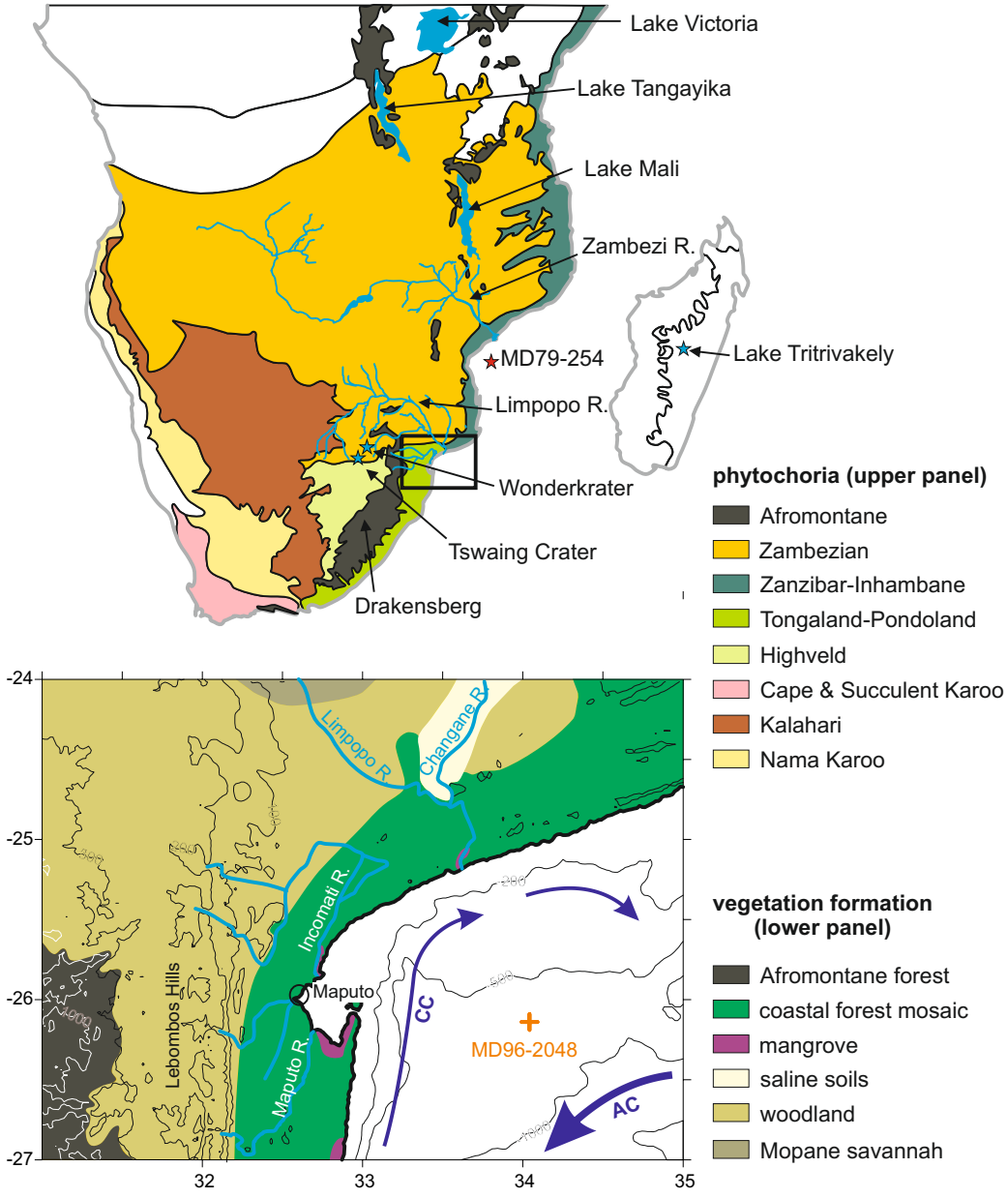

Fig. 1. Upper panel: map of southern Africa with the main phytochoria after White (1983). Location of sites mentioned in the text are denoted by asterix. Lower panel: site location of MD96-2048; main vegetation formations; main rivers; 100 m, 200 m, 500 m, and 1000 m contours; 200 m, 500 m, and 1000 m bathymetric contours; Agulhas (AC) and counter currents (CC) forming a coastal eddy. Zambezian vegetation woodland and savannah north of ∼25°30′ S, Tongaland-Pondoland coastal forests south of ∼25°30′ S, Zanzibar-Inhambane coastal forests east of 33–34° E. West of the escarpment with Afromontane forest rises the interior plateau covered with Highveld grasslands rises.

palm and termite savannah with *Hyphaene*, *Phoenix*, *Acacia*, *Garcinia*, *Cyperus*, *Phragmites* and other grasses (Kersberg, 1985, 1996).

Closed forest is found in the form of cloud forest (with a rich flora including *Podocarpus*) and semi-deciduous forest on the Drakensberg, riparian forest and coastal forest in the lowland, and mangroves along river estuaries. North of the site, in the Zambezian region, Miombo woodland (with *Brachystegia*) and Mopane dry woodland (with *Colophospermum mopane*) occur. Several types of woodland and scrubland with ticket or grass stratum are found in the lowlands west and northwest of the city of Maputo and on the Lebombos hills. Thicket also covers the littoral dunes. Woody savannahs occur in the higher parts along the Great Escarpment and the elevated inland plateau, the Highveld, is covered by open grasslands (Kersberg, 1985, 1996).

Along the coast north of the marine site, the littoral dunes are closely covered by evergreen hemi-sclerophyllous thicket. Behind the narrow coastal strip, closed forest in the form of evergreen seasonal to semi-deciduous lowland forest is found on the sub-littoral belt of ancient dunes. Behind the sub-littoral, Miombo woodland with *Brachystegia* grows northeast of the Limpopo River and comparable woodland, with *Sclerocarya* but without *Brachystegia* grows southwest of the river. Shrubland with *Combretum*, *Philenoptera*, *Ziziphus*, and *Acacia* exists between the Limpopo and Incomati Rivers. South and west of it, scrub savannah with *Acacia*, *Sclerocarya*, *Combretum*, *Ziziphus*, and *Peltophorum africanum* covers the lowland area west and east of the Lebombos hills (Kersberg, 1985, 1996).

4 Material and methods

The marine core MD96-2048 (26°10′ S 34°01′ E, Fig. 1) was retrieved by the Marion Dufresne cruise MOZAPHARE (MD 104) at 660 m water depth on the upper continental slope east of Maputo and south of the mouth of the Limpopo River. The shelf here is rather broad and the continental slope is not very steep. The southern directed flow of warm waters of the Agulhas Current system is structured in counter clockwise eddies except for the shallower area along the coast (Lutjeharms and da Silva, 1988). The clockwise current along the coast off Maputo forms an eddy, the flow of which slows in the centre where suspended material settles (Martin, 1981). Our site is located in the northern part of the southern Limpopo cone depot centre which has been built up since Late Miocene times (Martin, 1981).

The material was retrieved at 660 m water depth by giant piston coring. The age model of MD96-2048 is constructed by correlating the stable oxygen isotopes of the benthic foraminifer *Planulina wuellerstorfi* to the global reference stack LR04 (Lisiecki and Raymo, 2005; Caley et al., 2011). The oxygen isotope stratigraphy indicates a rather slow, but continuous sedimentation rate. For this study, 116 samples from the upper 6 m covering the past 342 Ka (MIS 9 to 1) have been palynologically analysed by the first author.

Samples of 3 to 7 ml were taken every two to five cm from the upper 6 m. Volume was measured using water displacement. Samples were decalcified with diluted HCl (∼12 %) and after washing, were treated with HF (∼40 %) for several days to remove silicates. Two *Lycopodium* spore tablets containing $10\,680 \pm 1.8$ % markers each were added during the decalcification step. Samples were sieved over a cloth with meshes of 8 µm (diagonal) using ultrasonic treatment, which resulted in the removal of particles smaller than 10–12 µm. When necessary the sample was decanted to remove remaining silt. Samples were stored in water, mounted in glycerol, and microscopically examined (magnification 400 and 1000x) for pollen, spores, and dinoflagellate cysts by the first author. Pollen (Table 1) was identified using Scott (1982b), the African Pollen Database http://medias3.mediasfrance.org/pollen/, and the reference collection of African pollen grains of the Department of Palynology and Climate Dynamics of the University of Göttingen.

Two types of time-series analysis were carried out: Wavelet analysis after Torrence and Compo (1998) and cross spectral analysis using AnalySeries 2.0 (Paillard et al., 1996). To create equidistant series for spectral analysis, endmember abundances were re-sampled every 3 Ka between 0 and 342 Ka. The Wavelet analysis applied a Mortlet 6.00 wavelet, zero padding, and a white-noise background spectrum http://paos.colorado.edu/research/wavelets/. Cross spectral analysis was performed after the Blackman-Tuckey method using a Bartlett Window with 35 lags resulting in a bandwidth of 0.0142857. Errors and coherency have been calculated for the 95 % confidence level (non-zero coherency > 0.554094; error estimate $0.486146 < \Delta$ Power/Power < 3.11201). To check the significance of the power maxima in the frequency domain, we used the f-test of the Multi-Taper-Method.

5 Results

5.1 Pollen concentration and percentages of selected pollen taxa

Percentages are calculated based on the total number of pollen and spores and selected curves are plotted in Figs. 2 and 3. The material varied strongly in the amount of palynomorphs. Therefore, not all samples could be counted to a desirable pollen sum of 300 or more. Most sums vary between 100 and 390 pollen and spores, but in a few cases not even 100 pollen and spores could be found. The calculation sum is depicted in Fig. 2. Percentages are based on the total of pollen and spores. The pollen concentration per ml and a summary diagram are given in Fig. 3. The age model (after Caley et al., 2011) is constructed by comparison of the stable oxygen isotope curve of benthic foraminifers to the stack of LR04 (Lisiecki and Raymo, 2005).

Pollen concentration per ml is rather low, mostly less than 2000 grains per ml and lower in the older part of the studied sequence between 340 and 120 Ka than in the younger part after 120 Ka. Maxima of more than 4000 grains per ml are found at depths dated around 115, 90, 70, and 60–40 Ka. After 40 Ka pollen concentrations are again low and decline further after 15 Ka (Fig. 3).

215 pollen taxa have been identified, 108 taxa turned up in more than 5 samples (Table 1). Most abundant pollen is from *Podocarpus* (yellow wood), Cyperaceae (e.g. sedges), and Poaceae (grasses). Pollen taxa have been grouped in pollen from (a) forest trees, (b) woodland trees and scrubs, (c) mountainous herbs, scrubs and trees, (d) coastal and halophytic scrubs and herbs, (e) riparian and swamp plants based on Kersberg (1996) and Coates

Table 1. List of grouped pollen taxa occurring in 5 or more samples. Grouping was done using Kersberg (1996) and Coates Palgrave (2002) The columns EM1, EM2, EM3 denote the scores (in percent) of the taxa on each of the endmember assemblage EM1, EM2, or EM3, respectively (highest scores in bold). r^2 is the coefficient of determination (n.s., not significant). See methods for details of the endmember modelling unmixing procedure (Weltje, 1997).

Pollen type	Family	EM1	EM2	EM3	r^2
Cyperaceae		18.98	**42.37**	28.26	0.39
Poaceae		7.63	14.04	**19.53**	0.42
Podocarpus	Podocarpaceae	**52.19**	18.02	10.14	0.66
	Asteraceae				
Asteroideae pp	Asteraceae	0.50	4.30	**4.35**	0.31
Cichorioideae pp	Asteraceae				n.s.
Cotula-type	Asteraceae	0.00	0.10	**0.68**	0.29
daisy-type	Asteraceae	0.18	**1.18**	0.71	0.10
Gazania-type	Asteraceae				n.s.
Pentzia-type	Asteraceae	0.00	0.77	**1.30**	0.18
Stoebe-type	Asteraceae	0.00	**1.18**	0.16	0.19
Tarchonanthus/Artemisia	Asteraceae				n.s.
Vernonia	Asteraceae				n.s.
	forest trees				
Buxus madagascaria-type	Buxaceae				n.s.
Celastraceae		0.00	0.02	**0.09**	0.04
Chrysophyllum	Sapotaceae	0.00	0.07	**0.25**	0.16
Crotalaria	Fabaceae	0.11	0.00	**0.16**	0.05
Garcinia	Clusiaceae	**0.26**	0.00	**0.26**	0.06
Hymenocardia	Euphorbiaceae	**0.33**	0.00	0.20	0.10
Ilex	Aquifoliaceae				n.s.
Khaya-type	Meliaceae	0.03	0.00	**0.51**	0.21
Lophira	Ochnaceae				n.s.
Macaranga	Euphorbiaceae				n.s.
Mallotus-type	Euphorbiaceae	1.24	0.06	**2.65**	0.17
Meliaceae/Sapotaceae					n.s.
Schizeaceae		**0.45**	0.38	0.00	0.04
Tetrorchidium-type	Euphorbiaceae?	0.00	**0.16**	0.14	0.08
Thymelaeaceae pp					n.s.
Zanthoxylum	Rutaceae				n.s.
	woodland trees and scrubs				
Acacia	Mimosaceae				n.s.
Acanthaceae pp		0.06	0.00	**0.26**	0.09
Alchornea	Euphorbiaceae	0.89	0.03	**3.69**	0.47
Balanites	Balanitaceae	0.08	0.08	**0.73**	0.18
Brachystegia	Caesalpiniaceae	0.01	0.11	**0.73**	0.13
Bridelia	Euphorbiaceae				n.s.
Burkea africana	Caesalpiniaceae	0.46	0.00	**0.66**	0.18
Cassia-type	Caesalpiniaceae	0.43	0.00	**1.04**	0.08
Celtis	Ulmaceae	**0.70**	0.00	0.21	0.11
Cleome	Capparaceae	0.07	0.00	**0.07**	0.07
Coffea-type	Rubiaceae				n.s.
Combretaceae pp		0.20	0.14	**1.14**	0.23
Croton	Euphorbiaceae				n.s.
Daniellia-type	Fabaceae	0.11	0.00	**0.42**	0.20
Diospyros	Ebenaceae				n.s.
Dodonaea viscosa	Sapindaceae	0.27	0.09	**0.77**	0.11
Dombeya	Sterculiaceae				n.s.
Dracaena	Agavaceae				n.s.

Table 1. Continued.

Pollen type	Family	EM1	EM2	EM3	r^2
Euclea	Ebenaceae				n.s.
Euphorbia	Euphorbiaceae	0.58	0.00	**1.32**	0.19
Fabaceae		0.18	0.00	**0.50**	0.09
Grewia	Tiliaceae				n.s.
Hyphaene	Arecaceae	0.07	**0.21**	0.07	0.04
Hypoestes-type	Acanthaceae				n.s.
Indigofera-type	Fabaceae	0.15	0.04	**0.30**	0.05
Klaineanthus	Euphorbiaceae				n.s.
Lannea/Sclerocarya	Anacardiaceae	0.03	0.00	**0.36**	0.12
Manilkara-type	Sapotaceae	0.58	0.00	**0.61**	0.13
Parinari	Chrysobalanaceae	0.04	0.00	**0.08**	0.05
Peltophorum africanum	Caesalpiniaceae	**0.15**	0.00	0.07	0.06
Philenoptera-type	Fabaceae				n.s.
Pterocarpus-type	Fabaceae				n.s.
Rhamnaceae pp					n.s.
Rhus	Anacardiaceae				n.s.
Rubiaceae pp		0.04	0.00	**0.13**	0.05
Sapotaceae pp					n.s.
Schrebera-type	Oleaceae	0.27	0.00	**0.65**	0.14
Sorindeia juglandifolia-type	Anacardiaceae				n.s.
Spermacoce	Rubiaceae	0.04	0.00	0.27	0.13
Tapinanthus	Loranthaceae				n.s.
Tarchonanthus/Artemisia	Asteraceae				n.s.
Tephrosia-type	Fabaceae				n.s.
Uapaca	Euphorbiaceae	0.08	**0.40**	0.20	0.05
Urtica-type	Urticaceae	**0.20**	0.00	0.00	0.08
mountainous herbs, scrubs and trees					
Aloe-type	Liliaceae	0.05	**0.34**	0.17	0.04
Anthoceros	Anthocerotaceae				n.s.
Anthospermum	Rubiaceae	0.27	0.29	**0.88**	0.07
Ericaceae		0.19	**6.23**	1.85	0.47
Lycopodium	Lycopodiaceae				n.s.
Lycopodium cernuum-type	Lycopodiaceae	0.04	**0.14**	0.00	0.05
Myrica	Myricaceae				n.s.
Myrsine africana	Myrsinaceae	**1.19**	0.00	1.11	0.14
Olea	Oleaceae				n.s.
Passerina	Thymelaeaceae	0.00	**0.80**	0.10	0.18
Phaeoceros	Anthocerotaceae	0.71	**1.79**	0.00	0.30
Protea/Faurea	Proteaceae	0.14	0.00	**0.20**	0.03
Pseudolachnostylis-type	Euphorbiaceae	0.14	0.00	**0.58**	0.19
Restionaceae		0.15	**0.52**	0.00	0.05
Stoebe-type	Asteraceae	0.00	**1.18**	0.16	0.19
mangrove tree					
Rhizophora	Rhizophoraceae	0.82	0.00	**1.11**	0.14
coastal and halophytic scrubs and herbs					
Aizoaceae		0.80	0.00	**0.82**	0.06
Boscia/Maerua	Capparaceae				n.s.
Caryophyllaceae pp					n.s.
Chenopodiaceae/Amaranthaceae		0.12	0.74	**2.17**	0.47
Gazania-type	Asteraceae				n.s.
Polycarpaea	Caryophyllaceae	**0.10**	0.00	0.06	0.05

Table 1. Continued.

Pollen type	Family	EM1	EM2	EM3	r^2
Raphia-type	Arecaceae				n.s.
Tribulus	Zygophyllaceae	0.03	0.19	**0.27**	0.04
Ziziphus-type	Rhamnaceae				n.s.
riparian and swamp plants					
Alismataceae pp		**1.94**	0.00	0.93	0.11
Borassus	Arecaceae				n.s.
Campanulaceae					n.s.
Phoenix	Arecaceae				n.s.
Polygonum senegalensis-type	Polygonaceae				n.s.
Pteris	Pteridaceae	**0.48**	0.13	**0.49**	0.04
Stipularia africana	Rubiaceae	0.00	**0.11**	0.04	0.04
Typha	Thyphaceae	0.26	**0.83**	0.27	0.05
not classified					
Cnestis-type	Conneraceae				n.s.
Evolvulus-type	Convolvulaceae				n.s.
Plantago	Plantaginaceae				n.s.
Solanum	Solanaceae				n.s.
stephanocolporate, striatoreticulate	Solanaceae?				n.s.

Palmgrave (2002). Asteraceae (without *Stoebe*-type and *Tarchonanthus*/*Artemisia*-type), Cyperaceae, Poaceae, *Podocarpus*, and *Rhizophora* (mangrove tree) pollen are not placed in one of the groups mentioned above. Percentages of selected pollen taxa and groups calculated on the basis of total of pollen and spores are given in Fig. 2.

Pollen of woodland scrubs and trees as well as forest trees show maximum percentages during marine isotope stages (MIS) 9, 7, 5, and 1. Three successively declining percentage maxima are found for MIS 5. Fern spore percentages vary between 4 and 16 % with maxima during early MIS 7, early MIS 5, and MIS 1. Pollen of coastal and halophytic scrubs and herbs is not abundant. Most of this pollen is found parallel to the forest maxima. Also *Rhizophora* pollen is not abundant with maxima during early MIS 9 and early MIS 5. *Podocarpus* pollen percentages show maxima during terminations and the cooler phases of MIS 7 and 5. Pollen of mountainous scrubs and trees, including Ericaceae (heather), has low percentages during most of MIS 9, 7, 5, and 1. Percentages for this group show maxima during MIS 8, 6, and 4–2. Poaceae pollen percentages run parallel to those of the mountainous group except for maxima in MIS 7, early MIS 5, and late MIS 1. Cyperaceae pollen is relatively abundant with percentages between 10 and 40 %. Minima are found in MIS 9 and early MIS 5. Pollen of other riparian and swamp plants has a conspicuous maximum just before 100 Ka (Fig. 2).

5.2 Endmembers

We carried out a multivariate analysis in the form of an endmember model unmixing procedure (Weltje, 1997), the statistics of which are specifically designed for the treatment of percentage data using a version of the unmixer algorithm programmed in MATLAB by Dave Heslop in 2008. Taxa occurring in at least 5 different samples (listed in Table 1) are used in the endmember modelling (total of 108 taxa and 116 samples). We used a model with three components (EM1, EM2, EM3) explaining over 93 % of the variance ($r^2 = 0.935$). Iteration was stopped at 1000 resulting in a convexity at termination of 1.92. The scores of the pollen taxa on the endmembers are given in Table 1.

The endmembers "consist" of a mixture of pollen and spore taxa, whereby the focus within each endmember clearly differs (Figs. 4–6, Table 1). EM1 is dominated by the variability in the *Podocarpus* pollen abundance. Other significant contributions to EM1 are of Schizaceae (tree ferns), Alismataceae, *Celtis*, *Hymenocardia*, *Peltophorum africanum*, and *Myrsine africana*. In EM2 Cyperaceae pollen fluctuations are dominant and the variability of Ericaceae pollen and *Phaeoceros* (hornwort) spores is important together with that of Asteroideae and Poaceae pollen. Other significant contributions are of *Stoebe*-type, *Passerina*, Restionaceae (cape reeds), *Typha* (cattail), and *Lycopodium cernuum* (clubmoss). A large number of pollen taxa from forest and woodland (*Alchornea*, Combretaceae, *Khaya*-type, etc.) and mangroves (*Rhizophora*) score on EM3. Also

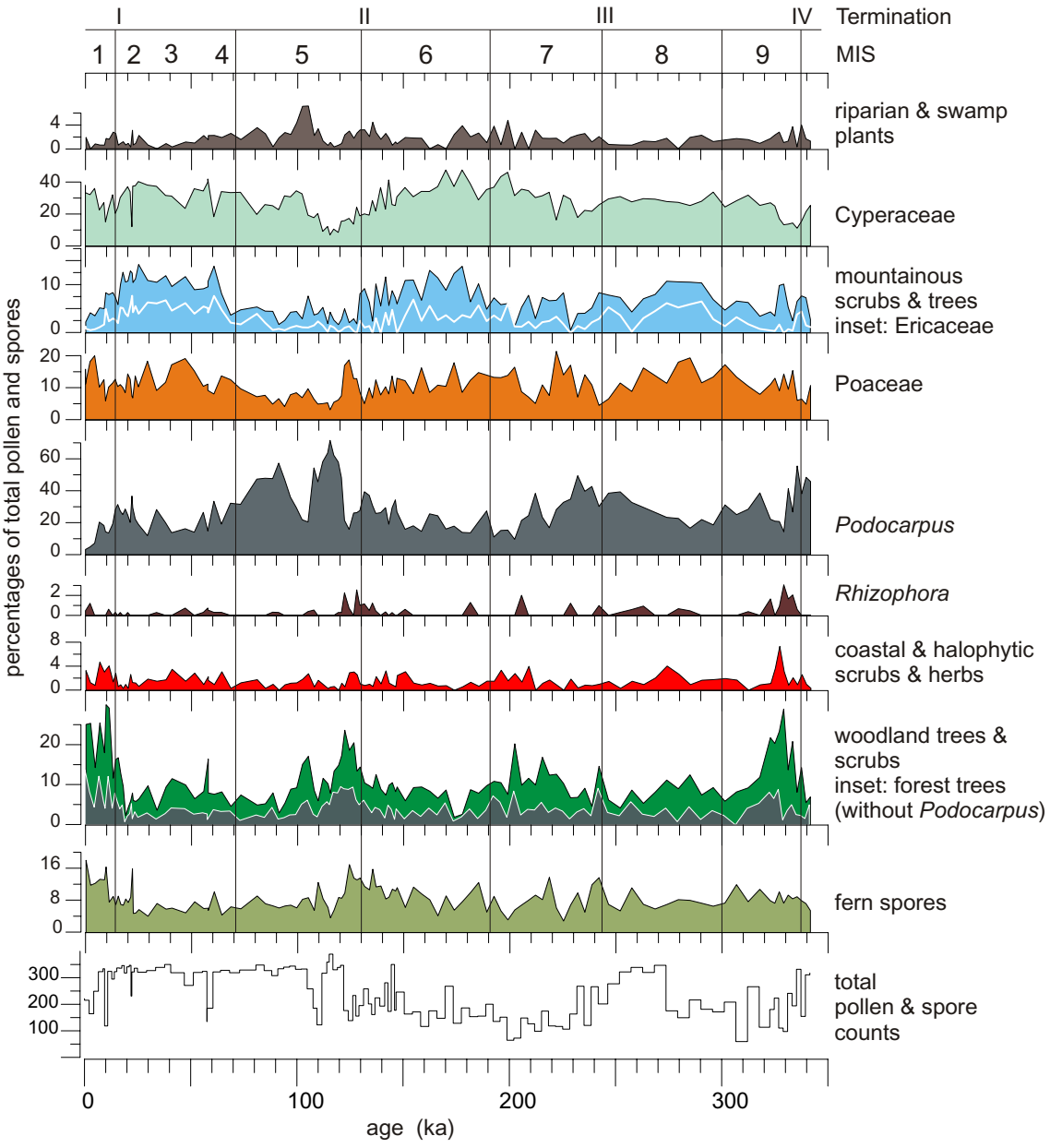

Fig. 2. Pollen percentages of groups (defined in Table 1) and selected taxa on the timescale of LR04 (Lisiecki and Raymo, 2005). Bottom curve shows the total of counted pollen and spores used in the percentage calculation. MIS, Marine Isotope Stage.

important for EM3 are the relative abundances of Chenopdiaceae/Amarantaceae, Poaceae, *Cotula*-type and other Asteroideae, and *Anthospermum* pollen.

The relative abundances of the endmembers plotted against time (Fig. 3) show a strong pattern of interglacial-glacial fluctuations, whereby EM3 is most abundant during interglacials (MIS 9, 7, 5e, and 1) and EM2 most abundant during glacials (MIS 8, 6, and 4 to 2). Additionally, EM3 reaches 0.4 during MIS 3 and short phases in MIS 6 and early MIS 8. EM1 scores during the intermediate periods.

6 Discussion

6.1 Source region of pollen and spores

Generally, the atmospheric circulation is not favourable for pollen transport to the marine site. Only Bergwinds and nightly land breezes (Tyson and Preston-Whyte, 2000) might carry pollen and spores directly from the Drakensberg and lowlands west of Maputo. On average, weak north and north-east winds might deliver pollen and spores during the late winter season. On the other hand, the site is situated less

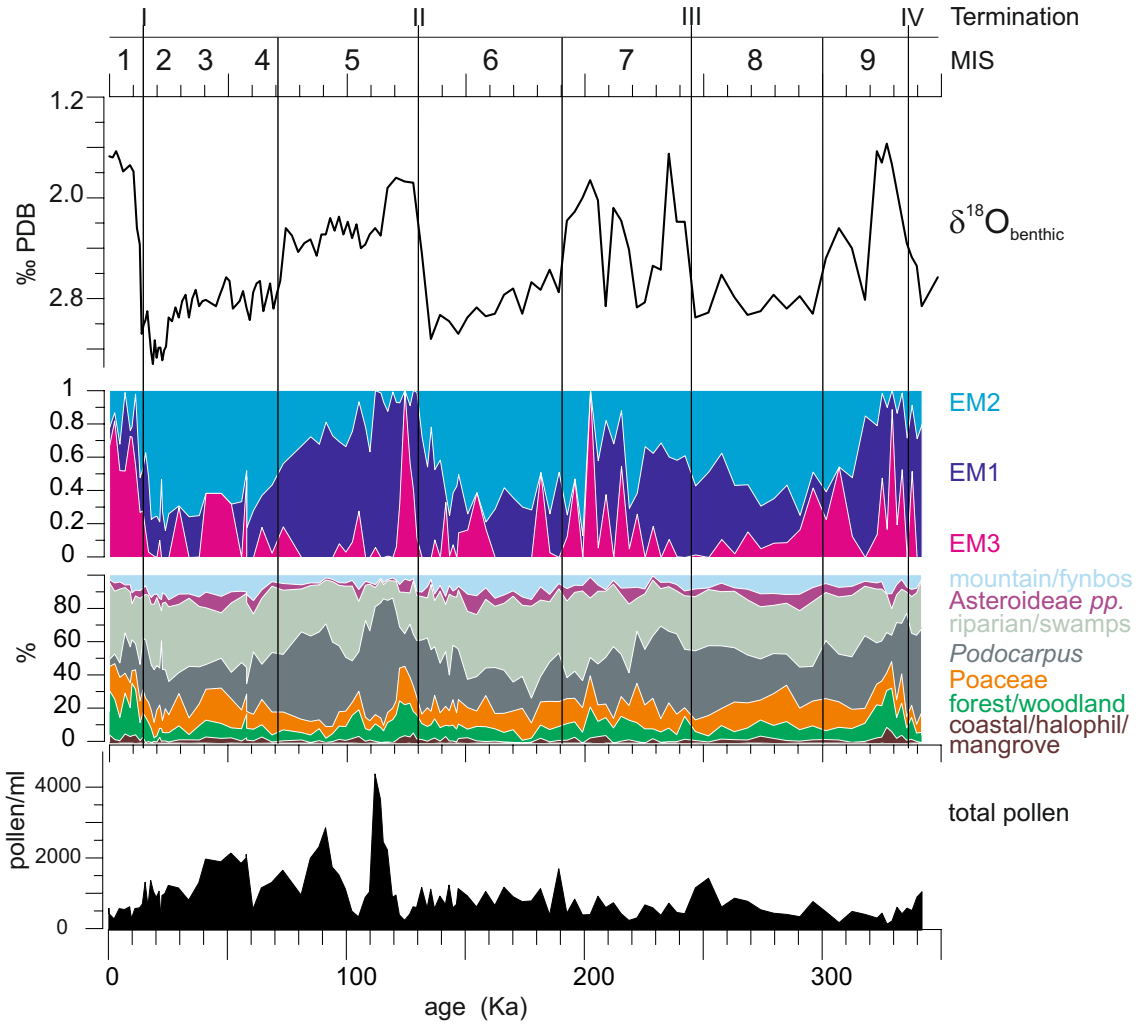

Fig. 3. Stable oxygen isotopes of benthic foraminifers per mille Pee Dee Belemnite (‰ PDB; Caley et al., 2011), cumulative Endmember abundances, summary pollen diagram (%), pollen concentration (ml^{-1}). MIS, Marine Isotope Stage.

than 120 Km from the coast and the mouth of the Limpopo River, the catchment of which covers a large area including parts of northern South Africa, Zimbabwe, and Mozambique. Because of the relative short distance to the coast and the location of the site on the southern Limpopo cone depot centre (Martin, 1981), we expect most pollen and spores to be fluvial. Therefore, the source region is probably mainly north of Maputo from the Drakensberg in the West to the coastal plain in the East. Results of organic geochemistry performed on the same sediments indicate that the relative amount of terrestrial soil material in the core is very low (Caley et al., 2011) and consequently the pollen concentration is also low.

6.2 Glacial-interglacial vegetation changes

The three endmembers, EM1, EM2, and EM3, being distinguished by the unmixer algorithm, can be interpreted as the representation of one or more vegetation complexes. EM1 (Fig. 4, Table 1) probably represents rather humid mountainous *Podocarpus* forest and combines *Podocarpus* values with values of woodland taxa such as *Peltophorum africanum* and *Celtis*, the Highveld taxon *Myrsine africana*, and taxa indicating moist conditions such as Alismataceae and tree ferns (Schizaceae). As *Podocarpus* values are the main constituent of EM1, *Podocarpus* pollen percentages and EM1 abundances show similar trends. However, it should be kept in mind, that *Podocarpus* is generally overrepresented by its pollen (Coetzee, 1967).

Types of humid mountain forests represented by pollen grouped in EM1 would have been more common – possibly also at lower altitudes – during MIS 9, MIS 7, and the later part of MIS 5. In the course of MIS 8, these forests became successively more important. Our pollen record suggests that periods of intermediate climate between full interglacial and full glacial, such as the cooler phases of MIS 5,

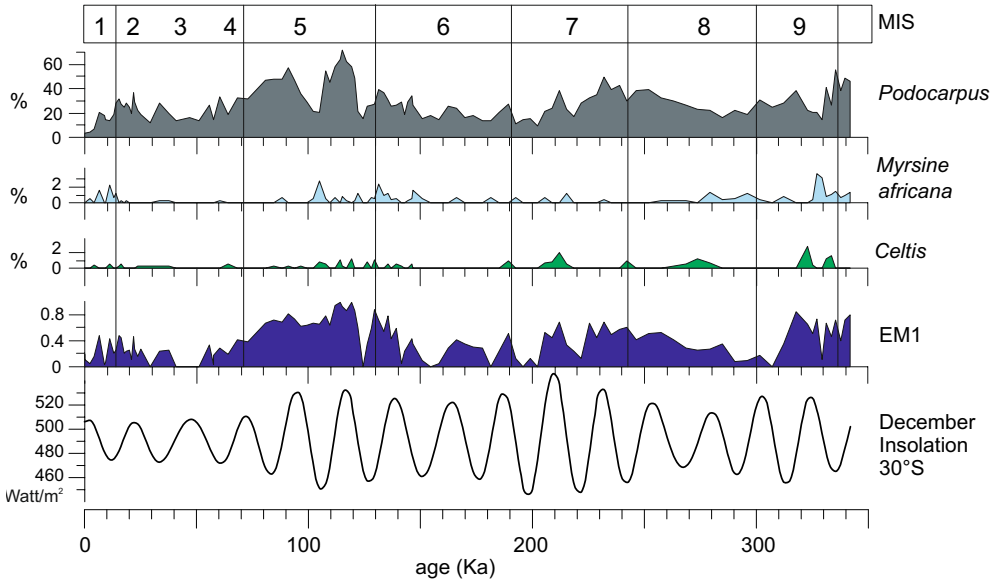

Fig. 4. Pollen percentages of selected taxa scoring relatively high on Endmember 1 (EM1). Bottom curve denotes the mean December insolation at 30° S after Laskar et al. (2004). MIS, Marine Isotope Stage.

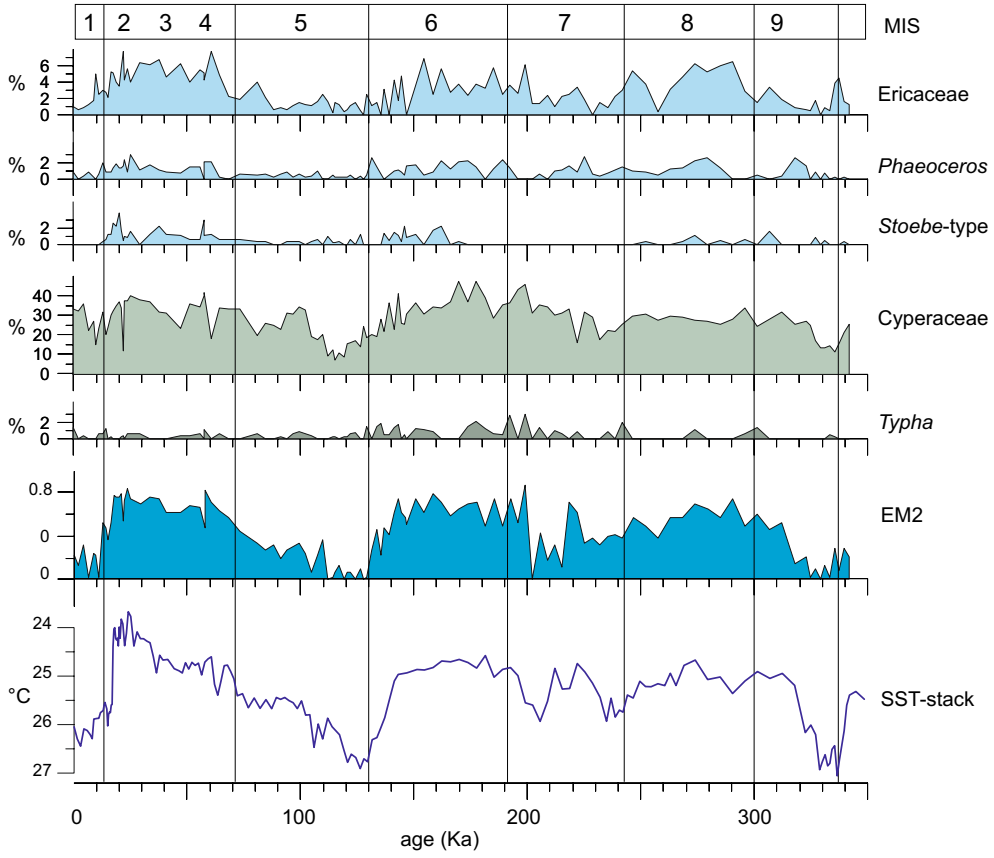

Fig. 5. Pollen percentages of selected taxa scoring relatively high on Endmember 2 (EM2), EM2 ratios, and SST-stack (Caley et al., 2011). Note the reversed Y-axis of the SST-stack. MIS, Marine Isotope Stage.

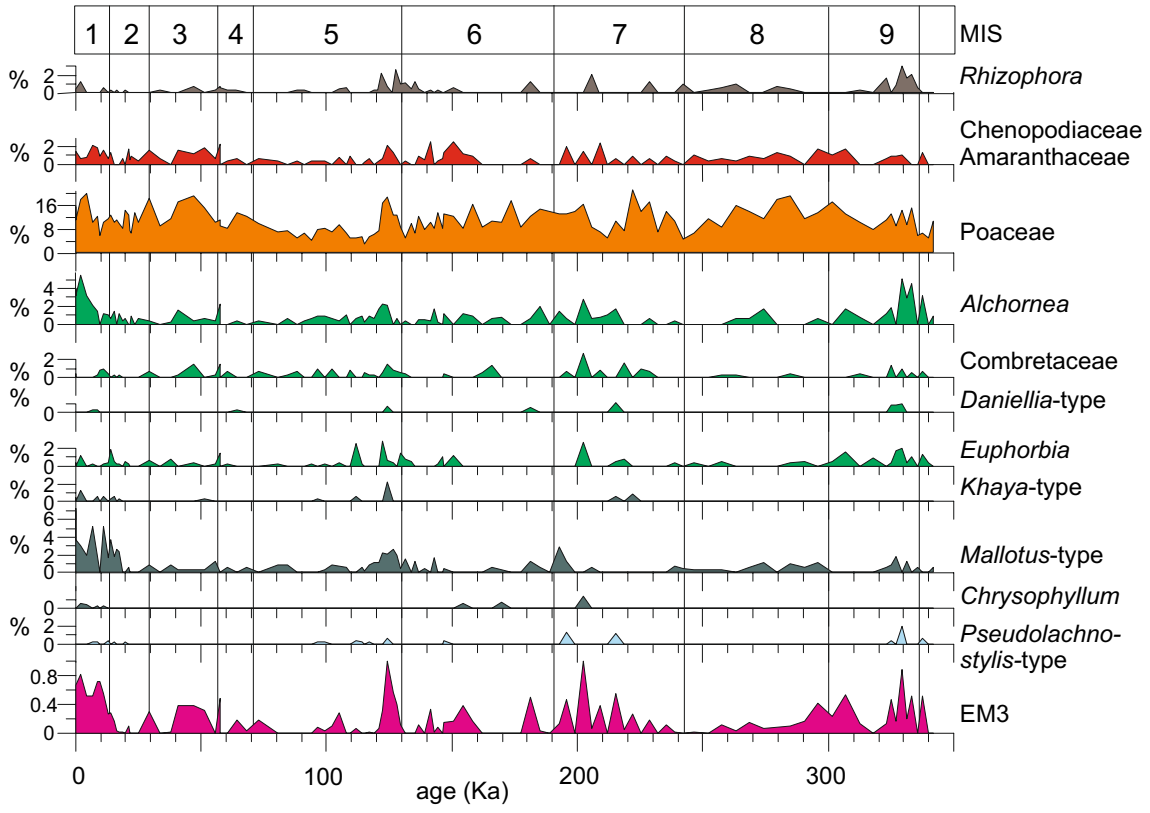

Fig. 6. Pollen percentages of selected taxa scoring relatively high on Endmember 3 (EM3). EM3 ratios at the bottom. MIS, Marine Isotope Stage.

were best suited for humid mountain forests. A combination of reduced temperatures and precipitation amounts that are comparable to modern values could have increased the net freshwater flux. During full glacial conditions, precipitation probably was less than today (e.g. Shin et al., 2003) and conditions might have been too dry for these forests even with reduced temperatures. During the Holocene the mountain forest was probably quite reduced.

EM2 (Fig. 5, Table 1) mainly represents the open mountain vegetation dominated by ericaceous scrubs (Ericaceae and some Asteroideae) together with a strong swampy component indicated by high scores of Cyperaceae, *Stipularia africana*, and *Typha*. Other mountain elements such as *Passerina*, *Stoebe*-type, and Restionaceae indicate fynbos-like vegetation (as found in high-altitude cool, wet parts of the Grassland Biome; Mucina and Rutherford, 2006). Furthermore hornwort (*Phaeoceros*) and clubmoss (*Lycopodium*) occur. EM2 is most abundant during full glacials (MIS 8, 6, 2 to 4), indicating that open mountainous habitats were common and had spread to lower altitudes. Woody vegetation and forest probably was sparse. Rivers could have been fringed with open swamps dominated by sedges and some grasses instead of gallery forest.

Compared to the record of the marine site MD79-254 situated in front of the Zambezi River (Van Campo et al., 1990), the maximum of Ericaceae pollen percentages in our record is slightly higher (7.8 % at the Limpopo compared to 5.7 % at the Zambezi) and that of Combretaceae lower (2.7 % instead of 8.0 %, respectively). The higher Ericaceae and lower Combretaceae relative pollen abundance at the southern site is consistent with a poleward decrease in temperatures.

EM3 combines pollen taxa from woodland and forest (Fig. 6, Table 1) with those of coastal vegetation, mangroves (*Rhizophora*), pioneer taxa (*Tribulus*), and halophytes (Chenopodiaceae/Amaranthaceae) on saline soils. *Anthospermum* and Poaceae from the Highveld grasslands are also represented. In combining such a variety of taxa, EM3 probably records a complex of different biomes not unlike the modern situation (see Sect. 3) with woodland and forest in the lowlands and grasslands on the interior plateau. This complex situation mainly occurred during full interglacial stages (MIS 9, 7, 5e, and 1).

6.3 Extent of the open mountain vegetation during glacials

A strong increase of mountain vegetation during glacials has also been found in other records of southern African

Table 2. Coherency (Coh.) and phase in degrees (φ) at orbital periodicities between endmembers and ETP (normalised and stacked eccentricity, obliquity, and negative precession), between EM1 and mean December insolation at 30° S (Ins.), and between EM2 and SST (Caley et al., 2011). At a confidence level of 95 %, coherence is non-zero if larger than 0.554. Phase is given in degrees in case of non-zero coherency.

	18.3 Ka		23 Ka		41 Ka		100 Ka	
	Coh.	φ[°]	Coh.	φ[°]	Coh.	φ[°]	Coh.	φ[°]
EM1 vs. ETP	0.78	140 ± 11	0.54		0.39		0.64	32 ± 16
EM2 vs. ETP	0.39		0.51		0.76	138 ± 11	0.82	205 ± 10
EM1 vs. Ins.	0.80	317 ± 10	0.54		0.32		0.15	
EM2 vs. SST	0.53		0.50		0.89	183 ± 7	0.98	173 ± 3

vegetation (e.g. Scott, 1982a, 1999; Gasse and Van Campo, 2001). West of the marine site MD96-2048, at Tswaing Crater (Scott, 1999; Scott and Tackeray, 1987) pollen from various vegetation types were found such as *Podocarpus* from mesic forest, Combretaceae, *Burkea africana*, and *Spirostachys* from warm savannah woodland, and *Tarchonanthus* probably from the dry savannah of the Kalahari "thornveld". During the glacial parts of the sequence *Artemisia*, *Stoebe*-type, *Passerina* and Ericaceae from cool or temperate shrubland and fynbos became important. Also in east South Africa, the sequence of Wonderkrater springs (Scott, 1982a) indicates a change from mostly cool upland vegetation types during the Glacial and the deglaciation to bushland during the Holocene, which is congruent with our results. According to the terrestrial evidence, the last Glacial vegetation included *Podocarpus* mesic forest and "bushveld" with Asteraceae, *Anthospermum*, *Cliffortia*, *Passerina*, Ericaceae, and *Stoebe* alternating with more open grassland communities. During the Holocene, a Kalahari type 'bushveld' with Combretaceae, Capparaceae, *Burkea africana*, *Acacia*, *Peltophorum africanum* and denser woodlands with *Olea* and Proteaceae occurred (Scott, 1982a).

A comparable pattern of glacial-interglacial vegetation changes is found on Madagascar recorded at Lake Tritrivakely (Gasse and Van Campo, 1998, 2001), where the glacial vegetation dominated by Ericaceae changed to a mosaic of open canopy vegetation (Poaceae, Asteraceae, Chenopodiaceae) alternated with woodland (*Celtis*, Combretaceae, *Macaranga*-type, *Uapaca*) or mountainous forest with *Podocarpus*, *Dombeya*, and *Vitex*. Putting the evidence of several pollen sequences in South Africa and Madagascar (Botha et al., 1992; Scott, 1982a, 1987, 1989, 1999; Gasse and Van Campo, 1998, 2001; Scott and Tackeray, 1987; Scott and Woodborne, 2007) together indicates that cool upland vegetation types, in the terminology of Scott (1999), might have dominated the moister uplands in southern African during glacial periods. It is comparable to the xerophytic woods and scrubs biome mapped by Elenga et al. (2000) as prominent in the Rift Valley during the Last Glacial Maximum.

6.4 Effects of SST of the Agulhas Current on the vegetation development

The pattern of vegetation change registered at MD96-2048, on the South African continent and on Madagascar suggests that glacial-interglacial cycles have had a strong impact on regional climates. The extension of the mountain vegetation might be the effect of lower temperatures and/or of low atmospheric CO_2 during the glacial. Glacial temperatures being 5–6 °C lower than today have been estimated by isotope studies on speleothems (Heaton et al., 1986; Stute and Talma, 1998; Holmgren et al., 2003). However, in case of the effects of low CO_2, also grasses should have increased, which is not found in our pollen record. Albeit a minor increase in Poaceae pollen percentages is found for MIS 8, 6, and 2 to 4, values remain under 20 % indicating no substantial increase of open savannah – let alone C_4 grass dominance – occurred in the region of the lower Limpopo River or in the Lebombos Hills. Other studies report a limited increase of C_4 grasses in South Africa related to colder and drier periods during MIS 4–2 (Holzkämper et al., 2009; Bar-Matthews et al., 2010; Chase, 2010).

Comparing the abundances of EM2 – open mountainous scrubland with fynbos affinities – with the stacked SST curve from our site (Caley et al., 2011), the correlation between the two is striking (Fig. 5). We performed a cross correlation between both curves showing coherency between SST and EM2 abundances at confidence levels exceeding 95 % for all periodicities longer than 25 Ka. SST and EM2 abundances are perfectly in anti-phase (Table 2), suggesting that development of mountain scrubland in southeast Africa is directly anti-correlated with the SST of the Agulhas Current. At present, the influence of the Agulhas Current is mainly through the increase of South African summer rainfall with increasing SST and vice versa (Jury et al., 1993; Reason and Mulenga, 1999). Our data indicate that this relation has been valid for at least the past 350 Ka covering several glacial-interglacial cycles.

The plants contributing to the EM2-signal are not specifically adapted to aridity but to cooler conditions, while Ericaceae and *Stoebe*-type also grow in much drier regions

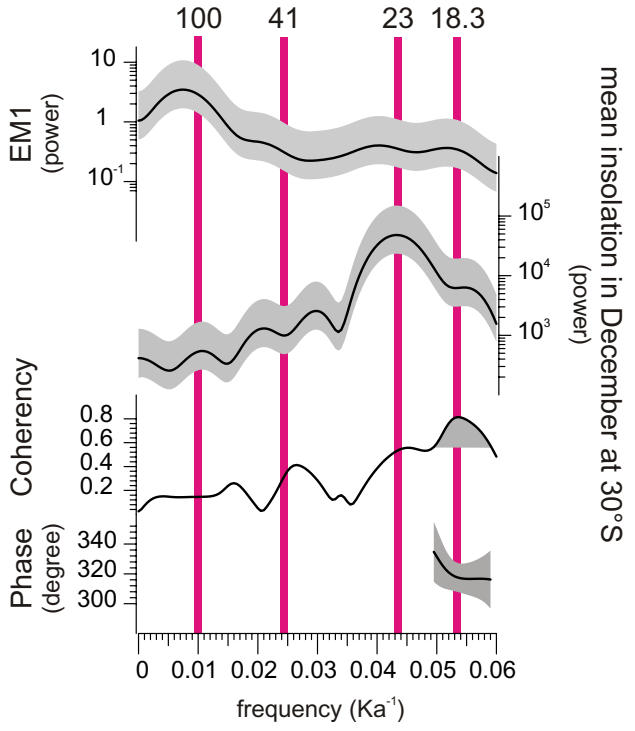

Fig. 7. Cross correlation between EM1 and mean December insolation at 30°S. From top to bottom: power spectra of EM1 (log scale left) and insolation (log scale right), coherency (non-zero coherency > 0.554, shaded), and phase in degrees. Confidence level is set at 95 %. Bandwidth is 0.014. Error ranges are shaded. Phase is only plotted if coherency is non-zero. Orbital periodicities in Ka are denoted by pink bars. At the 18 Ka precession band EM1 lags Southern Hemisphere December insolation by ∼40° (∼2 Ka). Interpolations and calculations were carried out in AnalySeries (Paillard et al., 1996).

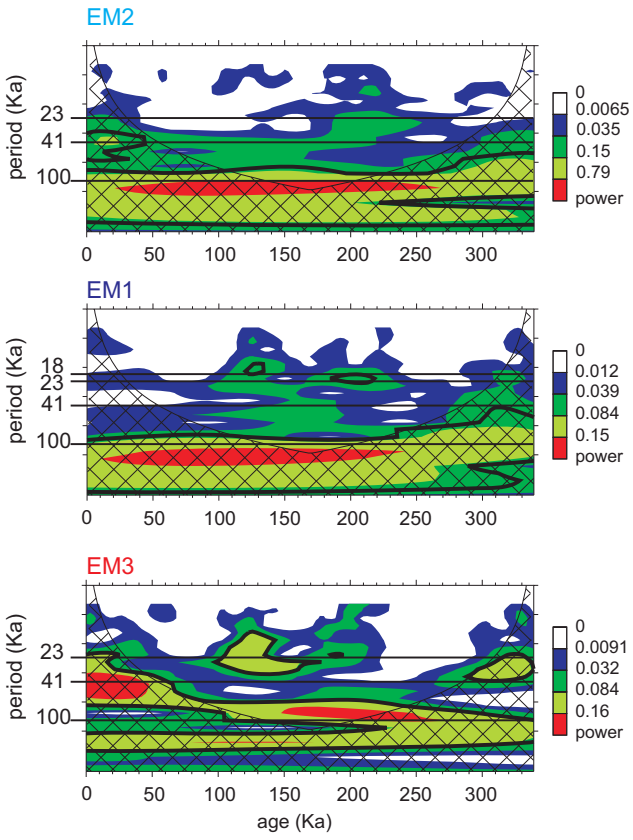

Fig. 8. Wavelet power spectra after Torrence and Compo (1998) for EM2 (top), EM1 (middle), EM3 (bottom). The contour levels are chosen so that 75 %, 50 %, 25 %, and 5 % of the wavelet power is above each level, respectively. The cross-hatched region is the cone of influence, where zero padding has reduced the variance. Black contour is the 90 % significance level, using a white-noise background spectrum.

than the present-day South African eastern Escarpment. The spread of mountainous vegetation indicates lower air temperatures during the glacial on one hand, while on the other, the correlation with lower SST suggests a relation between lower precipitation and glacial vegetation. Hence, we infer that lower temperatures combined with moderately less rainfall might have been the driver of the considerable extension of the mountain vegetation in eastern South Africa during glacials. Cooler and drier climate during glacials are consistent with results of coupled ocean-atmosphere models calculating air temperature over South Africa to have been lower by ∼3 to 4 °C during the Last Glacial Maximum (Bush and Philander, 1999; Shin et al., 2003). The SST of the southwestern Indian Ocean is modelled to have been 2 to 3 °C lower (Bush and Philander, 1999; Shin et al., 2003), while our SST-stack indicates maximally 3 °C lower SSTs during glacial periods (Caley et al., 2011). The resulting net freshwater flux between the Last Glacial Maximum and the present day changed little, because the reduced rainfall is offset by reduced air temperature (Bush and Philander, 1999).

6.5 Other influences on eastern South African vegetation and climate

Apart from the dominating glacial-interglacial variability, higher frequency rhythms are found in the vegetation record. To explore insolation forcing of the vegetation, we executed cross spectral analysis on the endmember abundances comparing them to the normalised and stacked eccentricity, obliquity, and negative precession (ETP). EM1 shows power coherent with ETP at the precession (although only at 18.3 Ka) and eccentricity bands, and EM2 shows coherency at the obliquity and eccentricity bands. The spectrum of EM3 is dependent of the other two. We give phase lags if coherency is non-zero (Table 2).

Comparing EM1 abundances to the local summer insolation (December, 30° S) suggests a positive response of the humid mountain forest to increased insolation (Fig. 4). The power spectrum of EM1 shows several significant maxima (between 143–103 Ka, at 49, 25, and 19 Ka), of which the

latter is coherent with insolation (Table 2, Fig. 7). The phase lag of 40° with the insolation maximum amounts to ca. 2 Ka. The wavelet analysis indicates that power in the precession band occurs mainly between 120–135 Ka and 190–220 Ka (Fig. 8), when precession variability in the insolation is large, which is a feature of tropical climates (Partridge et al., 1997; Trauth et al., 2003; Clement et al., 2004; Scholz et al., 2011).

It seems that the higher frequency variability in EM1 (humid mountain forest) is associated with local summer insolation, which is also in phase with Northern Hemisphere winter insolation as predicted by the model of Laepple and Lohmann (2009). Their study uses the regional seasonal variation to model glacial-interglacial temperature variability relying on the modern relationship between local insolation and temperature throughout the year. As the seasonal sensitivity to local insolation differs from region to region, Laepple and Lohmann (2009) distinguish between different temperature response regimes. The region of southern Africa south of ∼20° S is characterised by a summer precipitation maximum leading to evaporative cooling of the surface temperature which acts as a negative feedback with regard to temperature as a function of local insolation. Such a region has a higher temperature sensitivity in winter than in summer and is, therefore, called a winter sensitive area. The local response in a winter sensitive area at the Southern Hemisphere correlates to Northern Hemisphere insolation although driven by local insolation (Laepple and Lohmann, 2009).

The precessional component is rather weak in the pollen record. This might be the expression of the region being at the southern limit of the tropics. Of the monsoonal characteristics, it receives seasonal tropical rainfall but does not experience the seasonal change in wind direction (Leroux, 1983; Wang and Ding, 2008). According to Trenberth et al. (2000), the monsoon is explained by a vertical atmospheric structure of divergence in the upper troposphere and convergence in the lower troposphere. Southeastern Africa between 20° S and 30° S lies just south of the southernmost position of that atmospheric structure. The dominance of the glacial-interglacial variability in the record suggests that the monsoon did not have a strong impact during most of the past 300 Ka except for periods when eccentricity was strong and precession variability large.

EM2 abundances show significant power at 100 and 40 Ka that are explained by the tight fit of mountainous scrubland extension to SST variations in the western Indian Ocean (see previous section).

7 Conclusions

Pollen and spores have been retrieved from the upper part of core MD96-2048 covering the past 342 Ka. Although the pollen concentration is low due to the relative low terrestrial input to the marine site, the vegetation development in the region north and west of Maputo could be studied for three glacial/interglacial cycles.

The pollen record shows strong glacial-interglacial variability alternating three different complexes of vegetation formations; (i) woodland and forest in the lowlands with grasslands on the interior plateau during full interglacial periods, (ii) open mountainous scrubland with Fynbos affinities during most of each glacial, and (iii) mountainous *Podocarpus* forest and woodlands during cool and humid intermediate periods.

Comparison with SST estimates from the same core showed that the extension of the mountainous scrubland is tightly coupled to the Agulhas Current system. This is explained by the strong influence of western Indian Ocean surface temperatures on the summer precipitation in northern South Africa and southern Mozambique together with colder temperatures during glacial periods.

The variation of the mountainous forest record along with precession is associated with the effects of Southern Hemisphere summer insolation (at 30° S) on regional temperatures.

Acknowledgements. The authors want to thank Dave Heslop for making the unmixer algorithm available, Irina Nickeleit, Antje Kappel, Catalina Gonzalez, Annegret Krandick, and Sabrina Reinke for preparing the samples. The constructive comments of Louis Scott and an anonymous reviewer substantially improved the paper. The study was financially supported by the Deutsche Forschungsgemeinschaft (DFG). Data (pollen counts) are available at PANGAEA (www.pangaea.de).

Edited by: M. Siddall

References

Bar-Matthews, M., Marean, C. W., Jacobs, Z., Karkanas, P., Fischer, E. C., Herries, A. I. R., Brown, K., Williams, H.-M., Bernatchez, J., Ayalon, A., and Nilssen, P. J.: A high resolution and continuous isotopic speleothem record of paleoclimate and paleoenvironment from 90 to 53 ka from Pinnacle Point on the south coast of South Africa, Quaternary Sci. Rev., 29, 2131–2145, 2010.

Beuning, K. R. M., Zimmerman, K. A., Ivory, S. J., and Cohen, A. S.: Vegetation response to glacial–interglacial climate variability near Lake Malawi in the southern African tropics, Palaeogeogr. Palaeoclimatol., 303, 81–92, 2011.

Bonnefille, R. and Riollet, G.: The Kashiru pollen sequence (Burundi). Palaeoclimatic implications for the last 40,000 yr. B.P. in tropical Africa, Quaternary Res., 30, 19–35, 1988.

Botha, G. A., Scott, L., Vogel, J. C., and Von Brunn, V.: Palaeosols and palaeoenvironments during the Late Pleistocene Hypothermal in northern Natal, S. Afr. J. Sci., 88, 508–512, 1992.

Bush, A. B. G. and Philander, S. G. H.: The climate of the Last Glacial Maximum: Results from a coupled atmosphere-ocean general circulation model, J. Geophys. Res., 104, 24509–24525, 1999.

Caley, T., Kim, J.-H., Malaizé, B., Giraudeau, J., Laepple, T., Caillon, N., Charlier, K., Rebaubier, H., Rossignol, L., Castañeda, I.

S., Schouten, S., and Damsté, J. S. S.: High-latitude obliquity forcing drives the agulhas leakage, Clim. Past Discuss., 7, 2193–2215, doi:10.5194/cpd-7-2193-2011, 2011.

Chase, B.: South African palaeoenvironments during marine oxygen isotope stage 4: a context for the Howiesons Poort and Still Bay industries, J. Archaeol. Sci., 37, 1359–1366, 2010.

Chase, B. M. and Meadows, M. E.: Late Quaternary dynamics of southern Africa's winter rainfall zone, Earth-Sci. Rev., 84, 103–138, 2007.

Chase, B. M., Meadows, M. E., Carr, A. S., and Reimer, P. J.: Evidence for progressive Holocene aridification in southern Africa recorded in Namibian hyrax middens: Implications for African Monsoon dynamics and the "African Humid Period", Quaternary Res., 74, 36–45, 2010.

Clement, A. C., Hall, A., and Brocoli, A. J.: The importance of precessional signals in the tropical climate, Clim. Dynam., 22, 327–341, 2004.

Coates Palgrave, K.: Trees of Southern Africa, 3rd edition, revised and updated, Struik, Cape Town, 2002.

Coetzee, J. A.: Pollen analytical studies in east and southern Africa, Palaeoeco. A., 3, 1–146, 1967.

Cohen, A. S., Stone, J. R., Beuning, K. R. M., Park, L. E., Reinthal, P. N., Dettman, D., Scholz, C. A., Johnson, T. C., King, J. W., Talbot, M. R., Brown, E. T., and Ivory, S. J.: Ecological consequences of early Late Pleistocene megadroughts in tropical Africa, Proc. Natl. Acad. Sci., 104, 16422–16427, 2007.

Debusk, G. H.: A 37,500-year pollen record from Lake Malawi and implications for the biogeography of afromontane forests, J. Biogeogr., 25, 479–500, 1998.

Dupont, L.: Orbital scale vegetation change in Africa, Quaternary Sci. Rev., in press, 2011.

Elenga, H., Peyron, O., Bonnefille, R., Jolly, D., Cheddadi, R., Guiot, J., Andrieu, V., Bottema, S., Buchet, G., De Beaulieu, J.-L., Hamilton, A. C., Maley, J., Marchant, R., Perez-Obiol, R., Reille, M., Riollet, G., Scott, L., Straka, H., Taylor, D., Van Campo, E., Vincens, A., Laarif, F., and Jonson, H.: Pollen-based biome reconstruction for southern Europe and Africa 18,000 yr BP, J. Biogeogr., 27, 621–634, 2000.

Gasse, F. and Van Campo, E.: A 40,000-yr pollen and diatom record from Lake Tritrivakely, Madagascar, in the southern tropics, Quaternary Res., 49, 299–311, 1998.

Gasse, F. and Van Campo, E.: Late Quaternary environmental changes from a pollen and diatom record in the southern tropics (Lake Tritrivakely, Madagascar), Palaeogeogr. Palaeoclimatol., 167, 287–308, 2001.

Gasse, F., Chalié, F., Vincens, A., Williams, M. A. J., and Williamson, D.: Climatic patterns in equatorial and southern Africa from 30,000 to 10,000 years ago reconstructed from terrestrial and near-shore proxy data, Quaternary Sci. Rev., 27, 2316–2340, 2008.

Heaton, T. H. E., Talma, A. S., and Vogel, J. C.: Dissolved gas paleotemperatures and ^{18}O variations derived from groundwater near Uitenhagen, South Africa, Quaternary Res., 25, 79–88, 1986.

Heine, K.: The main stages of the late Quaternary evolution of the Kalahari region, southern Africa, Palaeoeco. A., 15, 53–76, 1982.

Holmgren, K., Lee-Thorp, J. A., Cooper, G. R. J., Lundblad, K., Partridge, T. C., Scott, L., Sithaldeen, R., Talma, A. S., and Tyson, P. D.: Persistent millennial-scale climatic variability over the past 25,000 years in Southern Africa, Quaternary Sci. Rev., 22, 2311–2326, 2003.

Holzkämper, S., Holmgren, K., Lee-Thorp, J., Talma, S., Mangini, A., and Partridge, T.: Late Pleistocene stalagmite growth in Wolkberg Cave, South Africa, Earth Planet. Sci. Lett., 282, 212–221, 2009.

Jury, M. R., Valentine, H. R., and Lutjeharms, J. R.: Influence of the Agulhas Current on summer rainfall along the southeast coast of South Africa, J. Appl. Meteorol., 32, 1282–1287, 1993.

Kersberg, H.: Afrika-Kartenwerk Serie S: Südafrika (Moçambique, Swaziland, Republik Südafrika), Bl. 7, Vegetationsgeographie, Gebrüder Bornträger, Berlin, 1985.

Kersberg, H.: Beiheft zu Afrika-Kartenwerk Serie S: Südafrika (Moçambique, Swaziland, Republik Südafrika), Bl. 7, Vegetationsgeographie, Gebrüder Bornträger, Berlin, 1996.

Kirsten, I., Fuhrmann, A., Thorpe, J., Roehl, U., and Oberhaensli, H.: Hydrological changes in Southern Africa over the last 200 Ka as recorded in lake sediments from Tswaing impact crater, S. Afr. J. Geol., 110, 311–326, 2007.

The area lies in the transition between Laepple, T. and Lohmann, G.: Seasonal cycle as template for climate variability on astronomical timescales, Paleoceanography, 24, PA4201, doi:10.1029/2008PA001674, 2009

Laskar, J., Robutel, P., Joutel, F., Gastineau, M., Correia, A. C. M., and Levrard, B.: A long-term numerical solution for the insolation quantities of the Earth, Astron. Astrophys., 428, 261–285, 2004.

Lee-Thorp, J. A. and Beaumont, P. B.: Vegetation and seasonality shifts during the Late Quaternary deduced from $^{13}C/^{12}C$ ratios of grazers at Equus Cave, South Africa, Quaternary Res., 43, 426–432, 1995.

Leroux, M.: Le climat de L'Afrique tropicale, texte and atlas, Champion, Paris, 1983.

Lisiecki, L. E. and Raymo. M. E.: A Pliocene-Pleistocene stack of 57 globally distributed benthic δ^{18}O records, Paleoceanography, 20, PA1003, doi:10.1029/2004PA001071, 2005.

Lutjeharms, J. R. E. and Da Silva, A. J.: The Delagoa Bight eddy, Deep-Sea Res., 35, 619–634, 1988.

Marean, C. W., Bar-Matthews, M., Bernatchez, J., Fischer, E., Goldberg, P., Herries, A. I. R., Jacobs, Z., Jerardino, A., Karkanas, P., Minichillo, T., Nilssen, P. J., Thompson, E., Watts, I., and Williams, H. M.: Early human use of marine resources and pigment in South Africa during the Middle Pleistocene, Nature, 449, 905–908, 2007.

Martin, A. K.: The influence of the Agulhas Current on the physiographic deveopment of the northernmost Natal Valley (S.W. Indian Ocean), Mar. Geol., 39, 259–276, 1981.

Mucina, L. and Rutherford, M. C.: The vegetation of South Africa, Lesotho and Swaziland. Strelitzia, 19. South African National Biodiversity Institute, Pretoria, 2006.

Partridge, T. C., DeMenocal, P. B., Lorentz, S. A., Paiker, M. J., and Vogel, J. C.: Orbital forcing of climate over South Africa: a 200,000-year rainfall record from the Pretoria Saltpan, Quaternary Sci. Rev., 16, 1125–1133, 1997.

Partridge, T. C., Scott, L., and Hamilton, J. E.: Synthetic reconstructions of southern African environments during the Last Glacial Maximum (21–18 kyr) and the Holocene Altithermal (8–6 kyr), Quatern. Int., 57–58, 207–214, 1999.

Paillard, D., Labeyrie, L., and Yiou, P.: Macintosh program per-

forms time-series analysis, EOS Transactions AGU, 77, 379, 1996.

Reason, C. J. C. and Mulenga, H.: Relationships between South African rainfall and SST anomalies in the Southwest Indian Ocean, Int. J. Climatol., 19, 1651–1673, 1999.

Scholz, C. A., Cohen, A. S., Johnson, T. C., King, J., Talbat, M. R., and Brown, E. T.: Scientific drilling in the Great Rift Valley: The 2005 Lake Malawi Scientific Drilling Project – An overview of the past 145,000 years of climate variability in Southern Hemisphere East Africa, Palaeogeogr. Palaeoclimatol., 303, 3–19, 2011.

Scott, L.: A late Quaternary pollen record from the Transvaal bushveld, South Africa, Quaternary Res., 17, 339–370, 1982a.

Scott, L.: Late Quaternary fossil pollen grains from the Transvaal, South Africa, Rev. Palaeobot. Palyno., 36, 241–278, 1982b.

Scott, L.: Pollen analysis of Hyena coprolites and sediments from Equus Cave, Tauung, Southern Kalahari (South Africa), Quaternary Res., 28, 144–156, 1987.

Scott, L.: Climatic conditions in Southern Africa since the last glacial maximum, inferred from pollen analysis, Palaeogeogr. Palaeoclimatol., 70, 345–353, 1989.

Scott, L.: Vegetation history and climate in the Savanna biome South Africa since 190,000 ka: a comparison of pollen data from the Tswaing Crater (the Pretoria Saltpan) and Wonderkrater, Quatern. Int., 57–58, 215–223, 1999.

Scott, L. and Tackeray, J. F.: Multivariate analysis of late Pleistocene and Holocene pollen spectra from Wonderkrater, Transvaal, S. Afr. J. Sci., 83, 93–98, 1987.

Scott, L. and Woodbone, S.: Pollen analysis and dating of Late Quaternary faecal deposits (hyraceum) in the Cederberg, Western Cape, South Africa, Rev. Palaeobot. Palyno., 144, 123–134, 2007.

Scott, L., Holmgren, K., Talma, A. S., Woodborne, S., and Vogel, J. C.: Age interpretation of the Wonderkrater spring sedmients and vegetation change in the Savanna Biome, Limpopo province, South Africa, S. Afr. J. Sci., 99, 484–488, 2003.

Shi, N., Schneider, R., Beug, H.-J., and Dupont, L. M.: Southeast trade wind variations during the last 135 kyr: evidence from pollen spectra in eastern South Atlantic, Earth Planet. Sci. Lett., 187, 311–321, 2001.

Shin, S.-I., Liu, Z., Otto-Bliesner, B., Brady, E. C., Kutzbach, J. E., and Harrison, S. P.: A simulation of the Last Glacial Maximum climate using the NCAR-CCSM, Clim. Dynam., 20, 127–151, 2003.

Stute, M. and Talma, A. S.: Glacial temperatures and moisture transport regimes reconstructed from noble gases and δ^{18}O, Stampriet Aquifer, Namibia, in: Isotope techniques in the study of environmental change, Proceedings series IAEA, Vienna, 307–318, 1998.

Stuut, J.-B., Crosta, X., Borg, K. van der, and Schneider, R.: Relationship between Antartic sea ice and southwest African climate during the late Quaternary, Geology, 32, 909–912, 2004.

Torrence, C. and Compo, G. P.: A Practical Guide to Wavelet Analysis, B. Am. Meteorol. Soc., 79, 61–78, 1998.

Trauth, M. H., Deino, A. L., Bergner, A. G. N., and Strecker, M. R.: East African climate change and orbital forcing during the last 175 kyr BP, Earth Planet. Sci. Lett., 206, 297–313, 2003.

Trenberth, K. E., Stepaniak, D. P., and Caron, J. M.: The Global Monsoon as seen through the Divergent Atmospheric Circulation, J. Climate, 13, 3969–3993, 2000.

Tyson, P. D. and Preston-Whyte, R. A.: The weather and climate of Southern Africa, Oxford University Press, Cape Town, 2000.

Van Campo, E., Duplessy, J. C., Prell, W. L., Barratt, N., and Sabatier, R.: Comparison of terrestrial and marine temperature estimates for the apst 135 kyr off southeast Africa: a test for GCM simulations of palaeoclimate, Nature, 348, 209–212 1990.

Vincens, A., Garcin, Y., and Buchet, G.: Influence of rainfall seasonality on African lowland vegetation during the Late Quaternary: pollen evidence from Lake Masoko, Tanzania, J. Biogeogr., 34, 1274–1288, 2007.

Wadley, L.: Announcing a Still Bay industry at Sibudu Cave, South Africa, J. Hum. Evol., 52, 681–689, 2007.

Wang, B. and Ding, Q.: Global monsoon: dominant mode of annual variation in the tropics, Dynam. Atmos. Oceans, 44, 165–183, 2008.

Weltje, G. J.: End-member modeling of compositional data: numerical-statistical algorithms for solving the explicit mixing problem, Math. Geol., 29, 503–549, 1997.

White, F.: The vegetation of Africa, Natural Rescourses Research, 20, UNESCO, Paris, 1983.